Parsec-scale Jets in AGN: Insights into the Location of the γ-Ray Emission from Geodetic VLBI, *Gaia* EDR3, and Fermi-LAT

S. Lambert[1], A. Pierron[1], H. Sol[2]

Abstract With the advent of the *Gaia* astrometry mission and the constantly improving geodetic VLBI program providing both optical and radio reference frames with precisions better than 0.1 mas, challenging questions arise about identifying which mechanisms are behind the optical emission as well as other emissions at higher energies, especially the γ-ray emission. We use data from *Gaia* EDR3, the radio ICRF3, and GeV fluxes from the Fermi-LAT 4FGL catalog for a sample of about 800 common active galactic nuclei (AGN), dominated by blazars (BL Lac and FSRQs). We investigate the general trends of such populations in terms of geometry, classification, color indices, and GeV emission.

Keywords Reference systems – quasars – technique: interferometrics – technique: *Gaia*

1 Introduction

The observations of the European Space Agency (ESA) *Gaia* astrometry mission (Prusti et al., 2016; Brown et al., 2016) launched in 2013. The constantly improving geodetic very-long-baseline-radio-interferometry (VLBI) program led mainly by the International VLBI Service for Geodesy and Astrometry (IVS, Nothnagel et al., 2017), unveiled the sub-milliarcsecond geometry of the radio and optical emissions of active galactic nuclei (AGN) that constitute the reference points of the celestial reference system. Recent studies, comparing absolute radio and optical astrometry, VLBI imaging, and photometric properties, allowed a first general picture. The radio centroids at 8, 22, and 32 GHz are close to each other (< 0.1 mas) and arranged in order of increasing frequencies towards the inside of the jet, i.e., towards the central black hole, in coherence with a frequency-dependent model of the jet plasma opacity (Lambert et al., 2021). Optical centroids are generally downstream in the jet and are often significantly distant from radio centroids by 0.1 mas to several mas (Kovalev et al., 2017; Plavin et al., 2019; Kovalev et al., 2020; Xu et al., 2021; Lambert et al., 2021). These optical centroids often coincide with a radio component in the jet, often stationary, and can have a high degree of linear polarization in radio and optics, testifying to a well-organized magnetic field typical of a synchrotron emission (Kovalev et al., 2020; Lambert et al., 2021). Conversely, when the *Gaia* centroid is upstream of the jet relative to the radio centroid, we have rather a weak optical polarization suggesting that we see the signature of the accretion disk (Plavin et al., 2019).

The link between the radio-optical geometry and the very high energy (VHE) emission remains unclear. The observed temporal correlation between spectral energy density (SED) in optical and γ suggests a common emission region and correlated mechanisms (e.g., Larionov et al., 2020). In some cases, VHE flares appear to be correlated with VLBI 'events' (variation of the radio core, emergence of a knot, or formation of a stationary knot). In 3C279, Abdalla et al. (2019) deduce that the emission zone is located beyond the broad line region (BLR). This prevents VHE γ photons from being absorbed by ambient background radiation (disk

1. SYRTE, Observatoire de Paris - Université PSL, CNRS, Sorbonne Université, LNE
2. LUTH, Observatoire de Paris - Université PSL, CNRS, Université Paris-Cité

and BLR flux). But this suggests a fairly large emission zone, difficultly explaining the very rapid (sometimes observed) variations. In practice, the observed variabilities remain difficult to reproduce with current 'standard' models, especially if we consider an emission zone far into the jet (and therefore a priori less compact than an area at the base of the jet).

Most of the studies used individual approaches on few well-studied sources. Interestingly, Kramarenko et al. (2022) recently proposed a global approach using hundreds of MOJAVE 15-GHz fluxes (Lister et al., 2018) and Fermi-Large Array Telescope (LAT, Abdollahi et al., 2020) γ fluxes. They suggest that the dominant high-energy production zone is typically located at a distance of several parsecs from the central nucleus, and that quasars have a more distant γ-ray emission region from the central engine and shorter variability time-scale compared to those of BL Lacertae (BL Lac) objects. The time-domain correlation between emission mechanisms at various wavelengths noticed in the above-cited works could have a spatial signature, as the γ emission region could be related in some cases to the optical photocenter observed by *Gaia*, i.e., an active zone emitting non-thermal radiation in the optical band and whose place in the jet can be probed by multiwavelength absolute astrometry. We explore that possibility in this paper by studying the radio-optical geometry of the sources and comparing it with their optical and VHE photometric properties.

2 Data and Their Preparation

Our radio catalog consists of the third realization of the international celestial reference frame (ICRF3, Charlot et al., 2020) restrained to the 4,536 entries at X-band (8.4 GHz). For the optical counterparts, we proceeded with a cross-matching of the full *Gaia* Early Data Release 3 (EDR3) positions (Prusti et al., 2016; Brown et al., 2021) with the ICRF3 positions with a cross-identification radius of 1 arcsecond. We found 3,516 sources with no statistically significant parallaxes. From *Gaia* EDR3, we also collect values for the BP-RP color index. BP-RP is the difference in magnitude between 330–660 nm (BP) and 630–1,000 nm (RP) bands and can usually be used as an indicator of which of the standard accretion disk or the synchrotron jet dominates the optical emission, the latter producing a redder luminosity, the former leading to a bluer source (see, e.g., Plavin et al., 2019).

We obtained the γ 1–100 GeV fluxes and their uncertainties from the Fermi Large Area Telescope (LAT) fourth source catalog data release 3 (4FGL-DR3, Abdollahi et al., 2020, 2022) for 816 sources of our sample. From the same catalog, we recorded the source classification, 488 of the sources being tagged as flat spectrum radio quasars (FSRQ) and another 214 being classified as BL Lac (see Figure 1). The remaining 114 sources are classified as three AGN, three compact steep-spectrum (CSS) radio sources, one Seyfert 1, 12 radio galaxies, one steep spectrum radio quasars (SSRQ), 92 blazar candidates of uncertain type (BCU), and one source of unknown type.

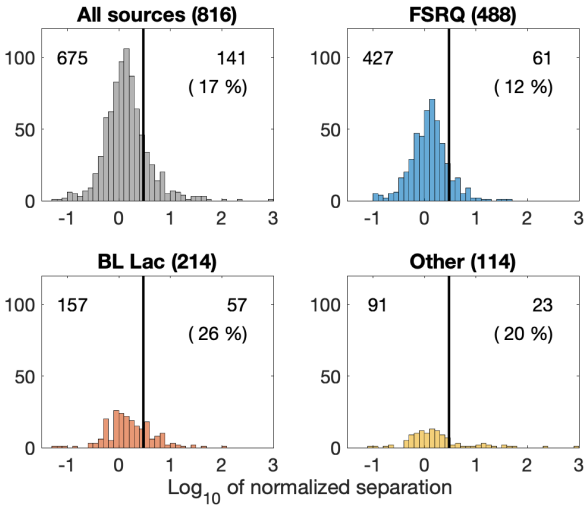

Fig. 1 Distribution of the radio-optical normalized separations (see, e.g., Mignard et al., 2016, about the computation of this quantity) of the source sample. The black, vertical line indicates a normalized separation of 3 (or a separation of 3σ).

Then, we form the radio-optical vector as the difference between the 8-GHz VLBI positions (referred to as X-band centroids) and the *Gaia* EDR3 positions (referred to as optical centroids). The uncertainty on the angular separation is computed using classical spherical astrometry formulae accounting for the correlation between estimates of right ascension and declination in both techniques (see, e.g., Mignard et al., 2016; Charlot et al., 2020). We assume for convenience that the X-band centroid can be considered as the radio core of the VLBI sources.

3 Analysis and Results

The obtained radio-optical angular separations are compared with the BP-RP color index and the γ flux in order to isolate general trends. The joint distributions of these three quantities is studied using several representations in Figures 2 and 3. In the upper plots of Figure 2 all sources are shown with different colors following the spectral class (FSRQ, BL Lac, other). Lower plots of Figure 2 are obtained by taking the medians of the y-axis quantity after dividing the x-scale in five bins containing an equal number of sources. The shaded area represents the standard error on the median. Figure 3 displays kernel smoothing density (KSD) of the distribution patterns of the different representations seen in the upper plots of Figure 2. The density is reported using a color scale from deep blue (less dense) to dark red (very dense) and is scaled for each plot: each map is saturated to its maximum level of density, the density plots intending to show where the sources are and not how many they are. The density is computed first for the whole sample of sources (upper row of Figure 3), then for sources whose radio-optical angular separation (denoted r) is larger or smaller than three times the cumulated uncertainty (σ) on the arc length (second and third rows of Figure 3), and finally for FSRQ and BL Lac (last two rows of Figure 3).

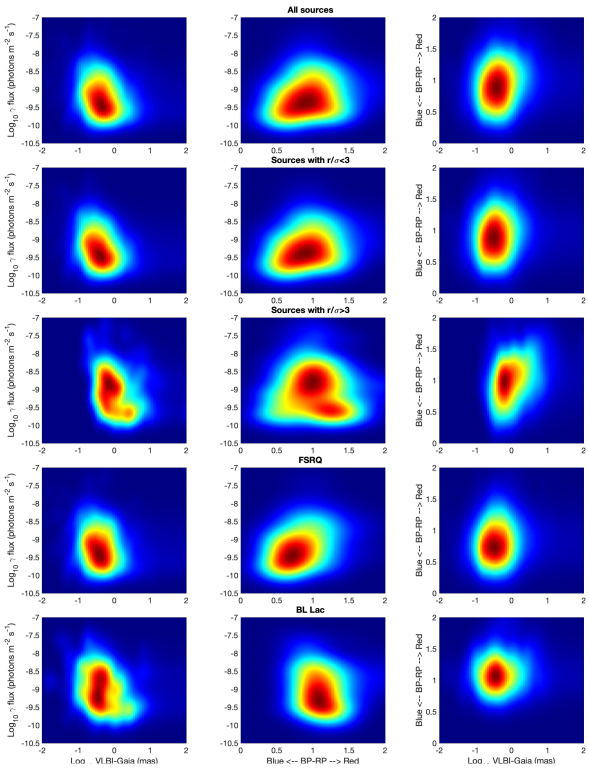

Fig. 3 Kernel smoothing density of distributions of Figure 2 for all sources of the sample (first row), for sources with not significant (second row) and significant (third row) radio-optical separation, for FSRQ (fourth row), and for BL Lac (fifth row).

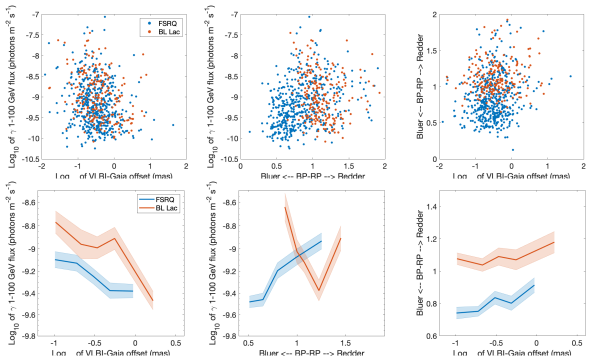

Fig. 2 Joint distributions of radio-optical angular separation, the BP-RP color index, and the γ flux. In the upper row, all sources are displayed. The plots in the lower row represent the median of the y-axis quantity in bins of the x-axis quantity containing equal numbers of sources. The shading gives the uncertainty on the median.

As the radio-optical angular separation increases, the BP-RP color index tends on average to become redder, suggesting that the corresponding optical sources are dominated by the jet, while sources exhibiting short radio-optical angular separations can have an optical emission affected by the presence of a disk. However, at low r such a trend seems mostly due to the FSRQ, which is coherent with the explanation by the bluer emission due to their standard accretion disk contributing to the optical emission located at low offset. For the population of BL Lacs, there is no signature of bluer emission at low r, which appears coherent with the presence of under-luminous accretion disks in such sources. Their BP-RP color index start to become redder only above an offset of about 0.6 mas, which can suggest a general cooling of the population of radiating particles propagating along the jets. Such an effect can also play a role in the case of the FSRQ at large offset, although the effect of the disk emission can dominate the optical radiation at low offset.

The LAT γ flux globally decreases as the radio-optical angular separation increases for the whole pop-

ulation, dominated by FSRQ. For the population of BL Lacs, the general trend is also a decrease of the γ-ray flux with the offset, but there is a clue of a flux enhancement for offset in the 0.3 to 0.6 mas range. Such an enhancement of the γ-ray flux for sources at intermediate r suggests the presence of an active zone along the jet which dominates both the optical and the γ-ray emission, likely related to one of the radio knots detected in most AGN mapped by VLBI. The highest γ fluxes of the whole population are coinciding with intermediate values of the color index, with an optimal value around BP-RP$\sim$1. Conversely, the bluest sources have the weakest γ fluxes, which can be expected if the accretion disk dominates their MWL emission, and the reddest sources have intermediate γ fluxes, suggesting that an active site in the jet boosts their emission at high energies.

Sources, for which the radio-optical angular separation is not—or poorly—significant ($r/\sigma < 3$), exhibit relatively blue color indices and weak γ fluxes. As shown in Figure 1, this population is dominated by FSRQ and these trends can be partially explained by the influence of the disk emission, which can dominate the optical flux and impose the small value of the radio-optical angular separation, but does not contribute to the γ-ray flux. Then the γ-rays have to come from some other active zone, either from the black hole magnetosphere, or from the jet base or some region downstream in the jet, and the optical counterpart of such non-thermal emission will also contribute to the total optical flux. However, the location of the current *Gaia* photocenter cannot help identifying the location of such non-thermal active site, as long as it is impossible to distinguish between the disk and the radio core positions. In contrast, the group of sources with significant radio-optical angular separations ($r/\sigma > 3$) show two subgroups: one with strong γ fluxes and mid color indices and one with weak γ fluxes and redder color indices, suggesting a weaker non-thermal activity. For these sources at large r, the optical emission fixes the *Gaia* photocenter position and cannot come from the accretion disk, nor from the immediate vicinity of the black hole, and neither from any spherical diffused halo around the central AGN engine. Although the presence of a diffuse asymmetric halo due to the host galaxy could affect the position of the optical photocenter, it is most likely dominated by some active zone(s) in the jet, coherent with their intermediate or redder color indices due to the expected synchrotron power-law jet emission in the optical range. Previous studies of a subsample of sources mapped by the MOJAVE program have shown that this is true for a large percentage of cases showing a spatial coincidence of the *Gaia* photocenter with a radio knot along the jet (Pierron et al., 2021, 2022). Such active non-thermal sites are the best candidates to emit as well the observed γ-ray flux by inverse-Compton processes. The presence of two subgroups is trickier to interpret but could be due to the existence of several active zones. For instance, the confinement shocks with decreasing activity along the jet, of which only the first two would appear in the study of the present AGN sample.

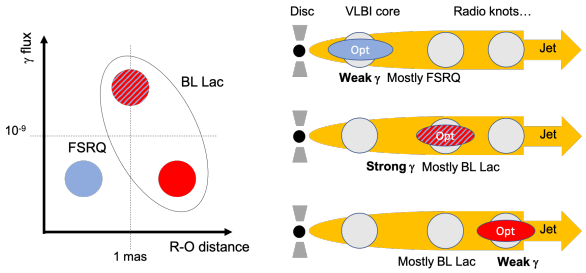

Fig. 4 (Left) Sketch representing the gross locations and color index of FSRQ and BL Lac in a representation following the radio-optical angular distance, the γ flux, and the BP-RP color index. The red (blue) indicates a redder (bluer) color index while the hatched disk means intermediates values of BP-RP. (Right) Sketch of the radio-optical-jet geometry corresponding to the three cases of the left sketch.

FSRQ globally exhibits bluer color indices that can be consistent with an optical emission arising from both the disk and the jet for appropriate parameters of the synchrotron emission. Their γ flux is weaker and is associated with shorter, non significant radio-optical angular separations. BL Lac color indices are globally redder than for FSRQ, consistently with an active jet and a weak disk. Within the BL Lac sample, one can again isolate two groups: (i) weak γ flux and high (red) color index associated with radio-optical angular separations around 1 mas or more, indicating an optical emission downstream in the jet, and (ii) strong γ flux for intermediate color index and relatively shorter radio-optical angular separations (0.1 to less than 1 mas), indicating an optical emission close to the VLBI core, possibly downstream but within the first parsec. The loci of the three cases (FSRQ, BL Lac group (i), BL Lac group (ii)) in the plane corresponding to the

radio-optical separation versus the γ flux are sketched in the left panel of Figure 4.

Interpreting the optical centroid as dominated by the non-thermal emission along the jet, it seems reasonable to associate this region with the γ emission zone for large radio-optical offsets when it is also associated with a radio knot. However, more work is needed to conclude about the position of the γ emission region for short radio-optical offsets. Indeed, it would need to distinguish the offset between the radio core and the optical center and therefore improve the absolute astrometry measurement within few tens of μas or less by reducing systematics of each technique and aligning rigorously the maps with the radio reference frame (that are, moreover, at different wavelengths).

4 Conclusion

In this study, we used two highest standards of absolute astrometry techniques—geodetic VLBI and *Gaia*—as well as photometric measurements including the results of the Fermi LAT spatial observatory. We showed the link between the γ flux and the location and color index of the optical centroid: globally weaker γ fluxes correspond to either FSRQ with short, non significant radio-optical offsets or BL Lac with radio-optical angular separations around 1 mas or more; in contrast, stronger γ fluxed are recorded for BL Lac with shorter but non-zero radio-optical offsets (0.1 to less than 1 mas), indicating an optical emission close to the VLBI core, likely downstream but within the first parsec.

As next steps that would improve our preliminary conclusions, it will be necessary to introduce redshifts and other individual characteristics of the sources, including more detailed classifications—in particular for LBL, IBL, and HBL in order to analyze possible trends in terms of blazar sequence—and geometrical parameters of jet (inclination) in order to consider the geometry in the frame of the source rather than in the one of the observer. The next *Gaia* releases and next ICRF versions—more observations, improved network, multifrequency—will reduce the systematics again, diminish the positional error, increase the sample, and allow to explore closer to the core. A coordination of the observing program of geodetic VLBI with other observations of AGN in the optical and γ (including ground-based photometric monitoring) would be welcome. From this synergy between astrogeodesy and astrophysics, we do expect that improving reference frames will improve the modeling of AGN jets and, conversely, that improving modeling of AGN jets will improve the reference frames.

Acknowledgements

This work has made use of data from the European Space Agency (ESA) mission *Gaia* (https://www.cosmos.esa.int/gaia), and processed by the *Gaia* Data Processing and Analysis Consortium (DPAC). Funding for the DPAC was provided by national institutions, in particular the institutions participating in the *Gaia* Multilateral Agreement. This research has made use of the NASA/IPAC Extragalactic Database (NED), which is funded by the National Aeronautics and Space Administration and operated by the California Institute of Technology.

References

Abdalla H, Adam R, Aharonian F, et al. (2019) Constraints on the emission region of 3C 279 during strong flares in 2014 and 2015 through VHE γ-ray observations with H.E.S.S. Astronomy & Astrophysics 627:A159

Abdollahi S, Acero F, Ackermann M, et al. (2020) Fermi large area telescope fourth source catalog. The Astrophysical Journal Supplement Series 247(1):33

Abdollahi S, Acero F, Baldini L, et al. (2022) Incremental fermi large area telescope fourth source catalog. The Astrophysical Journal Supplement Series, accepted for publication

Brown AGA, Vallenari A, Prusti T, et al. (2016) *Gaia* Data Release 1. Summary of the astrometric, photometric, and survey properties. Astronomy & Astrophysics 595:A2

Brown AGA, Vallenari A, Prusti T, et al. (2021) *Gaia* Early Data Release 3. Summary of the contents and survey properties. Astronomy & Astrophysics 649:A1

Charlot P, Jacobs CS, Gordon D, et al. (2020) The third realization of the International Celestial Reference

Frame by very long baseline interferometry. Astronomy & Astrophysics 644:A159

Kovalev YY, Petrov L, Plavin AV (2017) VLBI-*Gaia* offsets favor parsec-scale jet direction in active galactic nuclei. Astronomy & Astrophysics 598:L1

Kovalev YY, Zobnina DI, Plavin AV, Blinov D (2020) Optical polarization properties of AGNs with significant VLBI-*Gaia* offsets. Monthly Notices of the Royal Astronomical Society: Letters 493(1):L54

Kramarenko I, Pushkarev A, Kovalev Y, et al. (2022) A decade of joint MOJAVE-Fermi AGN monitoring: localisation of the gamma-ray emission region. Monthly Notice of the Royal Astronomical Society 510:469

Lambert S, Liu N, Arias EF, et al. (2021) Parsec-scale alignments of radio-optical offsets with jets in AGNs from multifrequency geodetic VLBI, *Gaia* EDR3, and the MOJAVE program. Astronomy & Astrophysics 651:A64

Larionov VM, Jorstad SG, Marscher AP, et al. (2020) Multiwavelength behaviour of the blazar 3C 279: decade-long study from γ-ray to radio. Monthly Notices of the Royal Astronomical Society 492(3):3829

Lister ML, Aller MF, Aller HD, et al. (2018) MOJAVE. XV. VLBA 15 GHz total intensity and polarization maps of 437 parsec-scale AGN jets from 1996 to 2017. Astronomical Journal 234(1):12

Mignard F, Klioner S, Lindegren L, et al. (2016) *Gaia* Data Release 1. Reference frame and optical properties of ICRF sources. Astronomy & Astrophysics 595:A5

Nothnagel A, Artz T, Behrend D, Malkin Z (2017) International VLBI Service for Geodesy and Astrometry. Journal of Geodesy 91(7):711

Pierron A, Lambert S, Sol H (2021) Insights into AGN parsec-scale emission from radio to GeV gamma rays from VLBI, *Gaia* EDR3, and Fermi-. Journées du Programme National des Hautes Energies, Paris, France

Pierron A, Lambert S, Sol H (2022) Parsec-scale jets in AGN: identification of the optical emission with radio knots. Astronomy & Astrophysics, in preparation

Plavin AV, Kovalev YY, Petrov LY (2019) Dissecting the AGN disk-jet system with joint VLBI-*Gaia* analysis. The Astrophysical Journal 871(2):143

Prusti T, de Bruijne JHJ, Brown AGA, et al. (2016) The *Gaia* mission. Astronomy & Astrophysics 595:A1

Xu MH, Lunz S, Anderson JM, et al. (2021) Evidence of the *Gaia*-VLBI position differences being related to radio source structure. Astronomy & Astrophysics 647:A189